

Article

A Two Fiber Bragg Gratings Sensing System to Monitor the Torque of Rotating Shaft

Yongjiao Wang ^{1,2}, Lei Liang ¹, Yinquan Yuan ^{1,*}, Gang Xu ¹ and Fang Liu ¹

Received: 19 December 2015; Accepted: 18 January 2016; Published: 21 January 2016

Academic Editor: Vittorio M. N. Passaro

¹ National Engineering Laboratory for Fiber Optic Sensing Technology, Wuhan University of Technology, Wuhan 430070, China; wangyongjiao@126.com (Y.W.); l30l30@126.com (L.L.); xugang524@163.com (G.X.); fangliu@whut.edu.cn (F.L.)

² School of Computer Science and Engineering, Henan University of Urban Construction, Pingdingshan 467000, China

* Correspondence: ymyyq@whut.edu.cn; Tel.: +86-27-8765-1850 (ext. 1107); Fax: +86-27-8765-1851

Abstract: By fixing two FBGs on the surface of a rotating shaft along the direction of $\pm 45^\circ$ and using dynamic wavelength demodulation technology, we propose an optical fiber sensing system to monitor the driving torque and torsion angle of the rotating shaft. In theory, the dependence relation of the dynamic difference of central wavelengths on the torque and torsion angle of the rotating shaft has been deduced. To verify an optical fiber sensing system, a series of sensing experiments have been completed and the measured data are approximately consistent with the theoretical analysis. The difference of two central wavelengths can be expressed as the sum of two parts: a “DC” part and a harmonic “AC” part. The driving torque or torsion angle is linear with the “DC” part of the difference of two central wavelengths, the harmonic “AC” part, meaning the torsion angle vibration, illustrates that periodic vibration torque may be caused by inhomogeneous centrifugal forces or inhomogeneous additional torques produced by the driving system and the load.

Keywords: fiber Bragg grating; rotating shaft; torque and torsion angle; vibration monitoring

1. Introduction

Rotating machinery, such as electromotors, generators, steam turbines, compressors and aviation engines, plays an important role in modern industrial development, and is also key equipment in military and civilian fields. The health status and faults of rotating machinery can be understood by monitoring the vibration signals of the rotating shaft of the rotating machinery, and the vibration signals of the rotating shaft are important indicators for equipment safety assessments [1]. In order to ensure the healthy running of rotating machinery, it is necessary to develop an efficient monitoring method. Electrical sensors, such as eddy-current sensors and inductive sensors are often used for the vibration measurement of rotating shaft, but electrical sensors are susceptible to electromagnetic interference [2].

Compared with electrical sensors, fiber Bragg grating (FBG) sensors have unique advantages such as immunity to electromagnetic fields, compatibility with harsh environmental conditions, multiplexing capabilities, high sensitivity, small volume, light weight and low noise. Therefore, FBGs are becoming widely used in health monitoring, vibration measurement, and other areas and are attracting more and more attention in diverse application [3–6]. Antunes proposed an L-shaped beam-based FBG sensor to monitor structure vibration [7], Weng constructed a diaphragm-based acceleration sensor for structure health monitoring [8], Liu presented a flat diaphragm-based FBG sensor to determine the vibration acceleration of a measured body [9], Wang proposed a non-contact magnetic coupling FBG sensor to achieve non-contact measurements of object displacement [10] and

Tan presented a non-contact vibration FBG sensor to monitor the vibration of rotating shafts [11]. Hwang and Lee proposed an online torsion sensing method using FBG sensors and an optical coupling method to monitor the torque of a rotating shaft [12,13], but the optical power measurement approach is susceptible to the interference of light loss caused by the relative movement of the optical coupler, moreover the quantitative relation between the optical power and torque was not shown. In this paper, based on the wavelength measurements of two FBGs by a high speed demodulator [14], we propose a system for monitoring the torque and torsion angle of rotating shafts, and we have completed a serial of vibration experiments, demonstrating that the measured data are identical with the simulated results.

2. Theory for the Wavelength Measurement of Two FBGs

The experimental scheme is illustrated in Figure 1. The system consists of a super light-emitting diode (SLED) (central wavelength ≈ 1550 nm, spectrum width ≈ 60 nm), a 3dB coupler, two FBGs (1[#]FBG and 2[#]FBG), a dynamic demodulator and a computer. The two FBGs are pasted along the 45° direction on the surface of the transmission shaft. Through the coupler, the light emitted from the SLED arrives at the gratings, and the reflected light from the two gratings is directed to the dynamic demodulator. Figure 2 is a sketch of the transmission shaft, whose diameter and length are denoted by D and L respectively. Under the action of pure torque M , the maximum shear strain occurs on the surface of the circular shaft and in the direction of 45° related to the axial direction:

$$\varepsilon = \frac{D}{2EI_p} M \quad (1)$$

where EI_p is torsional stiffness. Correspondingly, the torsion angle of the shaft with length L is:

$$\varphi = \frac{L}{GI_p} M \quad (2)$$

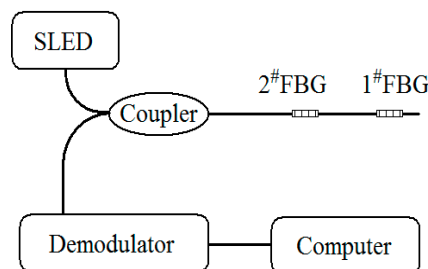


Figure 1. Experimental scheme.

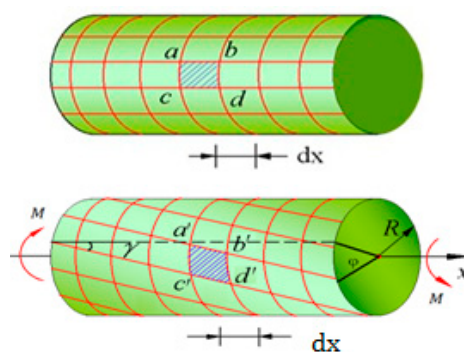


Figure 2. Sketch of the shaft torsion.

For a solid cylinder, using tensile elastic modulus G and Poisson's ratio μ , the shear elastic modulus G and inertia moment I_P can be expressed as:

$$G = \frac{E}{2(1 + \mu)} \quad (3)$$

$$I_P = \frac{\pi D^4}{32} \quad (4)$$

The reflection spectra of two FBGs undergoing dynamic uniform strain are symmetrical about their central wavelengths, and the dependence relationship of the wavelength on the strain and temperature change can be written as [3–6]:

$$\lambda_1(t) = \lambda_{10} + \lambda_{10}(1 - p_e)\varepsilon_1(z_{\text{mid}}, t) + \lambda_{10}[\zeta_s + (1 - p_e)(\alpha_s - \alpha_f)]\Delta T \quad (5)$$

$$\lambda_2(t) = \lambda_{20} + \lambda_{20}(1 - p_e)\varepsilon_2(z_{\text{mid}}, t) + \lambda_{20}[\zeta_s + (1 - p_e)(\alpha_s - \alpha_f)]\Delta T \quad (6)$$

where $\varepsilon_1(z_{\text{mid}}, t)$ and $\varepsilon_2(z_{\text{mid}}, t)$ are respectively the strains at the midpoints of two FBGs pasted along the direction of 45° on the surface of circular shaft as shown in Figure 3, so $\varepsilon_1(z_{\text{mid}}, t) = -\varepsilon$, $\varepsilon_2(z_{\text{mid}}, t) = \varepsilon$. ΔT is the temperature change, λ_{10} and λ_{20} are the initial wavelengths of two FBGs without the strain, $p_e = 0.22$ is the effective elasto-optic parameter of optical fiber. $\zeta_s = 6.45 \times 10^{-6}/^\circ\text{C}$ is the thermo-optic coefficient of fiber core, $\alpha_s = 11.6 \times 10^{-6}/^\circ\text{C}$ and $\alpha_f = 0.55 \times 10^{-6}/^\circ\text{C}$ are the linear expansion coefficients of fiber core and rotating shaft respectively. Taking $\lambda_{10} = 1540.619 \text{ nm}$ and $\lambda_{20} = 1555.791 \text{ nm}$, we obtained $\lambda_{10}[\zeta_s + (1 - p_e)(\alpha_s - \alpha_f)] = 23.37 \text{ pm}/^\circ\text{C}$ and $\lambda_{20}[\zeta_s + (1 - p_e)(\alpha_s - \alpha_f)] = 23.60 \text{ pm}/^\circ\text{C}$, so the effect of temperature change on the central wavelengths of two FBGs cannot be omitted for small strain, but the effect of temperature change on their difference is very little and can be omitted. Then the dynamic difference of central wavelengths of two FBGs undergoing dynamic linear strain is:

$$\Delta\lambda_{21}(t) = (\lambda_{20} - \lambda_{10}) + \lambda_{20}(1 - p_e)\varepsilon_2(z_{\text{mid}}, t) - \lambda_{10}(1 - p_e)\varepsilon_1(z_{\text{mid}}, t) \quad (7)$$

$$= (\lambda_{20} - \lambda_{10}) + (\lambda_{10} + \lambda_{20})(1 - p_e)\varepsilon \quad (8)$$

Considering Equations (1)–(4), we have:

$$\Delta\lambda_{21}(t) = (\lambda_{20} - \lambda_{10}) + (\lambda_{10} + \lambda_{20})(1 - p_e) \frac{D}{2EI_P} M(t) \quad (9)$$

and:

$$\Delta\lambda_{21}(t) = (\lambda_{20} - \lambda_{10}) + (\lambda_{10} + \lambda_{20})(1 - p_e) \frac{D}{4(1 + \mu)} \frac{\varphi(t)}{L} \quad (10)$$

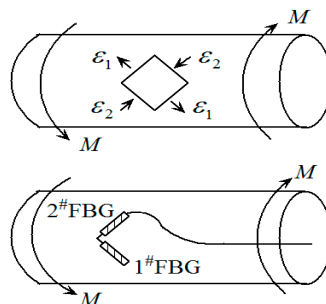


Figure 3. Two FBGs pasted along the maximum strain of the shaft torsion.

Equations (9) and (10) show that the wavelength difference is linear with the torque and torsion angle. Since our experiments show that the wavelength difference vibrates periodically with time, so we can suppose that the torsion angle of shaft obeys the simple harmonic vibration too:

$$\varphi(t)/L = \varphi_{DC} + \varphi_m \sin(2\pi ft + \phi_0) \quad (11)$$

$$M(t) = M_{DC} + M_m \sin(2\pi ft + \phi_0) \quad (12)$$

where φ_{DC} is the “DC” part of the torsion angle, φ_m is the maximum of the “AC” part of the torsion angle, M_{DC} is the “DC” part of the torque, M_m is the maximum of the “AC” torque, and they have the following relationship:

$$M_{DC} = GI_p \varphi_{DC}, \quad M_m = GI_p \varphi_m \quad (13)$$

Defining two factors:

$$K_\varphi = (\lambda_{10} + \lambda_{20}) (1 - P_e) \frac{D}{4(1 + \mu)} \quad (14)$$

$$K_M = (\lambda_{10} + \lambda_{20}) (1 - P_e) \frac{D}{2EI_p} \quad (15)$$

Then we have the following relationships about the dynamic difference of central wavelengths of two FBGs:

$$\Delta\lambda_{21}(t) = \Delta\lambda_{DC} + \Delta\lambda_m \sin(2\pi ft + \phi_0) \quad (16)$$

where the “DC” part and the maximum of “AC” part are respectively:

$$\Delta\lambda_{DC} = (\lambda_{20} - \lambda_{10}) + K_\varphi \varphi_{DC}, \quad \Delta\lambda_m = K_\varphi \varphi_m \quad (17)$$

or be expressed by the torque:

$$\Delta\lambda_{DC} = (\lambda_{20} - \lambda_{10}) + K_M M_{DC}, \quad \Delta\lambda_m = K_M M_m \quad (18)$$

Progressively, the “DC” part of torque M_{DC} comes from two parts, one is the driving torque, and the other is the friction torque between the shaft and the bearings:

$$M_{DC} = M_f + M_d \quad (19)$$

thus the central wavelength difference of two FBGs undergoing driving torque can be denoted by:

$$\Delta\lambda_{DC}(M_d) = \Delta\lambda_{DC}(0) + k_M M_d \quad (20)$$

$$\Delta\lambda_{DC}(0) = (\lambda_{20} - \lambda_{10}) + k_M M_f \quad (21)$$

3. Experimental Setup and Results

Figure 4 shows the basic experimental setup. The power is provided by a stepping motor, and the rotation speed of the shaft may be adjusted by the transducer. The load is provided by a magnetic powder brake and its torque can be changed from 0 to 3.4 Nm by adjusting the input current (0–0.45 A). Between the motor and the load we have installed a torque-speed sensor which can measure the torque and rotation speed. The optical system consists of two FBGs connected in series, a 3 dB coupler, and a SLED. A fiber optic rotary joint was used to transmit the light between the optical fiber at the shaft and the optical fiber on the ground. Through the coupler, the light emitted from the SLED arrives at the dual FBGs. For the wavelength demodulation scheme, the reflected light from the two gratings is directed to a high-speed demodulation instrument to monitor the dynamic Bragg wavelength of the two FBGs. The high-speed demodulation instrument (sm130 optical sensing interrogator, Micron

Optics, Inc. Atlanta, GA, USA) can measure the peak wavelengths of two FBGs with a resolution of 1 pm and sampling frequency of 1 kHz.

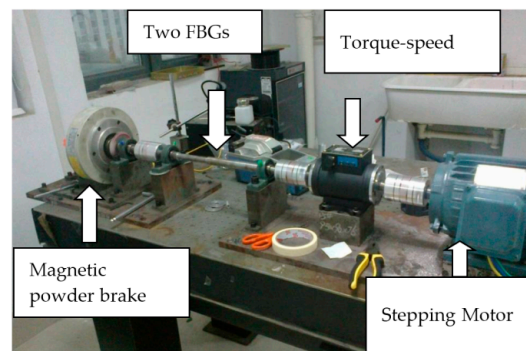


Figure 4. Experimental setup.

We prepared two FBGs (denoted as 1[#]FBG and 2[#]FBG) with different initial wavelengths, and as shown in Figure 3, pasted them on the surface of the circular shaft and in the direction of $\pm 45^\circ$ relative to the axial direction, respectively. Without any strain, their initial wavelengths are $\lambda_{10} = 1540.619$ nm and $\lambda_{20} = 1555.791$ nm, the wavelength difference of 15 nm ensures the separation of the two reflection peaks in the monitoring process. First, we have completed a series of experiments to account for the effect of the driving torque, where the rotating speed of 960 r/min is fixed. Figure 5 gives the typical central wavelengths of two FBGs with time for two torques (0 and 1.5 Nm). It can be seen that the central wavelengths of 1[#]FBG and 2[#]FBG follows an approximate sine change with time shown by Equation (16), and their vibrating maximum $\Delta\lambda_m$ are almost the same and the phase difference is about π ; the deviations are because the two FBGs are not pasted strictly in the $\pm 45^\circ$ direction.

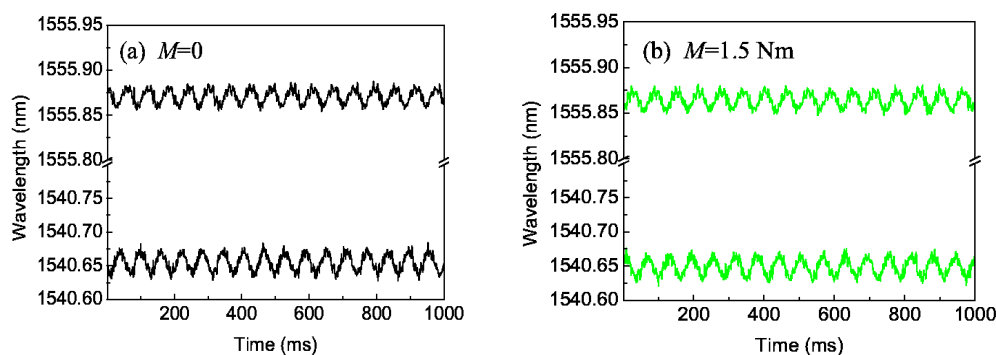


Figure 5. Central wavelengths of two FBGs with time: (a) $M = 0$; (b) $M = 1.5$ Nm.

Figure 6a gives the values of $\Delta\lambda_{DC}$ corresponding to different driving torques (0, 0.75, 1.5, 2.25 and 3.0 Nm) by squares, whereby one can see that these squares are nearly on one line. Substituting Equation (4) into Equation (15) and using the parameters of the shaft (45 steel, $E = 210$ GPa, $D = 20$ mm), we can obtain the theoretical value $k_M = 7.684$ pm/Nm in Equations (15), (18) and (21), and the line in Figure 6 was drawn according this slope. Noting that $\Delta\lambda_{DC}(0) = 15.207$ nm and $\lambda_{20} - \lambda_{10} = 15.172$ nm, we can obtain that their difference $\Delta\lambda_{DC}(0) - (\lambda_{20} - \lambda_{10}) \approx 32$ pm comes from the friction torque between the shaft and bearings, so we calculate the values of $\Delta\lambda_{DC}(M_d) - \Delta\lambda_{DC}(0)$ for the nonzero driving torque M_d as shown in Figure 6b, and it can be seen that the experimental data is approximately consistent with the theoretical analysis and $\Delta\lambda_{DC}(M_d) - \Delta\lambda_{DC}(0)$ is proportional to the driving torque. The deviation mainly comes from two reasons: One is because the two FBGs are not pasted strictly in the $\pm 45^\circ$ direction; the other is the error in driving torque caused by the current which controls the magnetic powder brake.

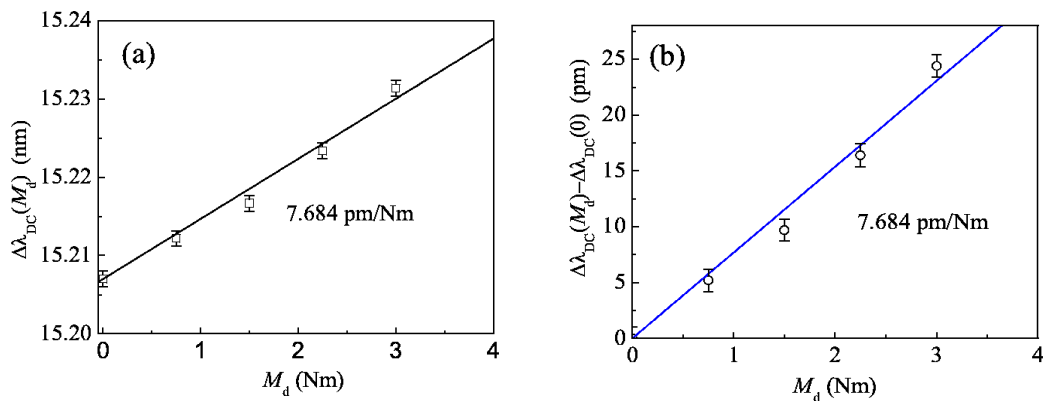


Figure 6. Central wavelength *versus* driving torque: (a) $\Delta\lambda_{DC}(M_d)$; (b) $\Delta\lambda_{DC}(M_d) - \Delta\lambda_{DC}(0)$.

Then, we have investigated the effect of the rotation speed, where the torque is fixed. Figure 7a–c gives the typical central wavelengths of two FBGs with time for three rotation speeds (420, 700, 960 and 1200 rpm), where the lower wavelength-time curve is $\lambda_1(t)$ of 1[#]FBG, the upper wavelength-time curve is $\lambda_2(t)$ of 2[#]FBG, and f_1 is the 1-order frequency of the fast Fourier transform for the vibration signal. We found that the values of $\Delta\lambda_{DC}$ and $\Delta\lambda_m$ are almost the same and the vibrating frequency of $\Delta\lambda_1(t)$ and $\Delta\lambda_2(t)$ increases with increasing rotation speed.

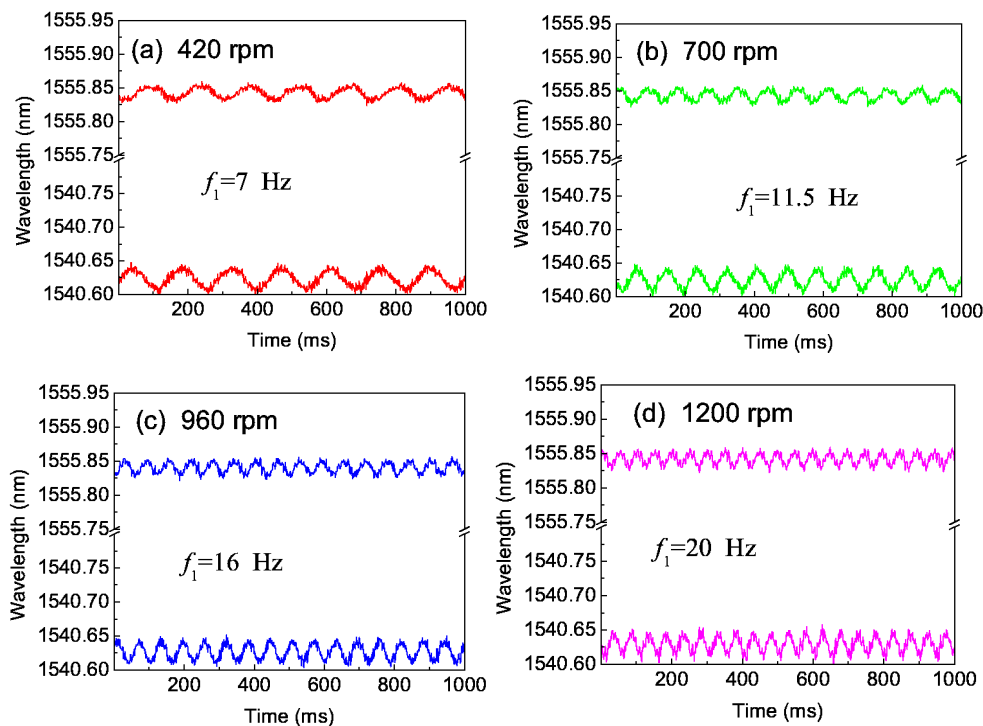


Figure 7. Central wavelengths of two FBGs with the time for four rotation speeds: (a) 420; (b) 700; (c) 960 and (d) 1200 rpm.

Figure 8 gives the vibration frequency values corresponding to four different rotation speeds (420, 700, 960, 1200 rpm) by squares, the line was drawing according to the formula $f_1 = n/60$. We found that the 1-order vibration frequency equals the rotation frequency of the shaft (within 1500 rpm), and the twist vibration of the shaft may be due to the inhomogeneous shaft mass distribution or the inhomogeneous additional torques produced by the driving system and the load.

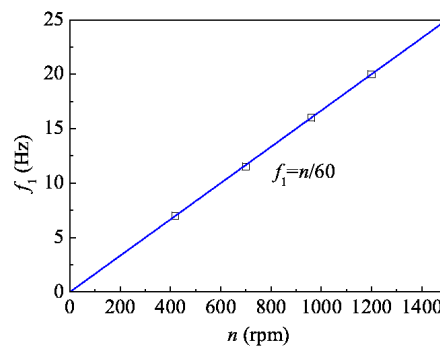


Figure 8. 1-order frequency of vibration signal *versus* rotating speed.

4. Conclusions

We have proposed an optical fiber sensing system for the torque and torsion angle of rotating shafts using two FBGs and high-speed wavelength demodulation. The dependence relationship of the dynamic difference of central wavelengths of two FBGs pasted on the surface of the circular shaft along the $\pm 45^\circ$ direction on the torque and torsion angle of the rotating shaft have been obtained. A serial of vibration experiments shows that the measured data are approximately consistent with the theoretical analysis. The difference of two central wavelengths can be divided into two parts: A “DC” part and a harmonic “AC” part. The “DC” part of the difference of two central wavelengths shows a good linear fit with the driving torque and the 1-order frequency of the harmonic “AC” part increases with the increasing rotation speed.

Acknowledgments: Supported by the Natural Science Foundation of Hubei Province, China (No. 20141j015), the National Science Foundation of China (No. 61402345), the Scientific and Technological Research Projects in Henan Province of China (No. 152102210092).

Author Contributions: Yongjiao Wang and Gang Xu finished all experiments, Lei Liang provided research platform, Fang Liu finished figure drawing and Yinquan Yuan finished the theoretical part and paper writing.

Conflicts of Interest: The authors declare no conflict of interest.

References

- Basumallick, N.; Biswas, P.; Dasgupta, K.; Bandyopadhyay, S. Design optimization of fiber Bragg grating accelerometer for maximum sensitivity. *Sens. Actuators A* **2013**, *194*, 31–39. [[CrossRef](#)]
- Todd, M.D.; Johnson, G.A.; Althouse, B.A.; Vohra, S.T. Flexural beam-based fiber Bragg grating accelerometers. *IEEE Photonics Technol. Lett.* **1998**, *10*, 1605–1607. [[CrossRef](#)]
- Berkoff, T.A.; Kersey, A.D. Experimental demonstration of a fiber Bragg grating accelerometers. *IEEE Photonics Technol. Lett.* **1996**, *8*, 1677–1679. [[CrossRef](#)]
- Kruger, L.; Swart, P.L.; Chtcherbakov, A.A.; van Wyk, A.J. Non-contact torsion sensor using fibre Bragg gratings. *Meas. Sci. Technol.* **2004**, *15*, 1448–1452. [[CrossRef](#)]
- Zhou, W.; Dong, X.; Shen, C.; Zhao, C.L.; Chan, C.C.; Shum, P. Temperature-independent vibration sensor with a fiber Bragg grating. *Microw. Opt. Technol. Lett.* **2010**, *52*, 2282–2285. [[CrossRef](#)]
- Kalenik, J.; Pajak, R. A cantilever optical-fiber accelerometer. *Sens. Actuators A* **1998**, *68*, 350–355. [[CrossRef](#)]
- Antunes, P.F.D.C.; Lima, H.F.T.; Alberto, N.J.; Rodrigues, H.; Pinto, P.M.F.; de Lemos, P.J.; Nogueira, R.N.; Varum, H.; Costa, A.G.; de Brito Andre, P.S. Optical fiber accelerometer system for structural dynamic monitoring. *IEEE Sens. J.* **2009**, *9*, 1347–1354. [[CrossRef](#)]
- Weng, Y.; Qiao, X.; Feng, Z.; Hu, M.; Zhang, J.; Yang, Y. Compact FBG diaphragm accelerometer based on L-shaped rigid cantilever beam. *Chin. Opt. Lett.* **2011**, *9*, 22–25.
- Liu, Q.; Qiao, X.; Zhao, J.; Jia, Z.; Gao, H.; Shao, M. Novel fiber Bragg grating accelerometer based on diaphragm. *IEEE Sens. J.* **2012**, *12*, 3000–3004. [[CrossRef](#)]
- Wang, J.; Liu, B.; Zhang, F.; Jiang, D. Non-contact magnetic coupling fiber Bragg grating displacement sensor. *Nanotechnol. Precis. Eng.* **2008**, *6*, 468–472.

11. Li, T.; Tan, Y.; Zhou, Z.; Cai, L.; Liu, S.; He, Z.; Zheng, K. Study on the Non-Contact FBG Vibration Sensor and Its Application. *Photonic Sens.* **2015**, *5*, 128–136. [[CrossRef](#)]
12. Hwang, Y.; Lee, J.M. Online Non-contact torsion sensing method using fiber Bragg grating sensors and optical coupling method. In Proceedings of the 2007 14th ICSV, Cairns, Australia, 9–12 July 2007.
13. Lee, J.M.; Hwang, Y. A novel online rotor condition monitoring system using fiber Bragg grating (FBG) sensors and a rotary optical coupler. *Meas. Sci. Technol.* **2008**, *19*, 065303–065307. [[CrossRef](#)]
14. Gangopadhyay, T.K. Prospects for Fiber Bragg Gratings and Fabry-Perot Interferometers in fibre-optic vibration sensing. *Sens. Actuators A* **2004**, *113*, 20–38. [[CrossRef](#)]



© 2016 by the authors; licensee MDPI, Basel, Switzerland. This article is an open access article distributed under the terms and conditions of the Creative Commons by Attribution (CC-BY) license (<http://creativecommons.org/licenses/by/4.0/>).